

Decision-Theoretic Meta-Learning: Versatile and Efficient Amortization of Few-Shot Learning

Jonathan Gordon*

Department of Engineering
University of Cambridge
jg801@cam.ac.uk

John Bronskill*

Department of Engineering
University of Cambridge
jfb54@cam.ac.uk

Matthias Bauer

University of Cambridge
Max Planck Institute for Intelligent Systems
bauer@tue.mpg.de

Sebastian Nowozin

Microsoft Research
Cambridge, UK
Sebastian.Nowozin@microsoft.com

Richard E. Turner

Department of Engineering
University of Cambridge
Microsoft Research
ret26@cam.ac.uk

This paper develops a general framework for data efficient and versatile deep learning. The new framework comprises three elements: 1) Discriminative probabilistic models from multi-task learning that leverage shared statistical information across tasks. 2) A novel Bayesian decision theoretic approach to meta-learning probabilistic inference across many tasks. 3) A fast, flexible, and simple to train amortization network that can automatically generalize and extrapolate to a wide range of settings. The VERSA algorithm, a particular instance of the framework, is evaluated on a suite of supervised few-shot learning tasks. VERSA achieves state-of-the-art performance in one-shot learning on Omniglot and *miniImageNet*, and produces compelling results on a one-shot ShapeNet view reconstruction challenge.

1. Introduction

Many applications, such as personalization and recommendation systems, require predictions to be made on myriad small, but related datasets. It is therefore critical to support *data efficient learning* through an ability to integrate diverse information sources. These same applications often also require *versatile learning* by which we mean fast and seamless adaptation to new and evolving situations (such as the addition of new classes and tasks), and an ability to do this in many settings (classification, regression, unsupervised learning etc.). Despite recent advances,

*Authors contributed equally.

notably in few-shot learning and meta-learning (Schmidhuber, 1987; Thrun and Pratt, 2012), deep learning lacks general purpose tools for data-efficient versatile learning.

This paper develops a versatile and data-efficient deep learning framework by incorporating three key elements. First, we leverage shared statistical structure between tasks via probabilistic models developed for multi-task and transfer learning. Probabilistic modeling provides a very general approach, but it requires careful integration with the deep learning toolbox. Second, we share information between tasks about how to learn using meta-learning (Naik and Mammone, 1992; Thrun and Pratt, 2012; Schmidhuber, 1987). Since uncertainty is rife in small datasets, we provide a new framework for meta-learning probabilistic inference using Bayesian decision theory. The framework provides a principled basis for recent episodic training schemes (Vinyals et al., 2016; Ravi and Larochelle, 2017), wherein each episode contains an internal train/test split. Third, we enable fast learning that can flexibly handle a wide range of tasks and learning settings via amortization (Kingma and Welling, 2014; Rezende et al., 2014). Typically amortization trades flexibility for speed, but we develop a novel architecture that also supports versatile learning.

The VERSA algorithm, a particular instance of the framework, is evaluated on a suite of supervised few-shot learning tasks. These provide an ideal test bed as they require data-efficiency (low-shot) and versatility (when adapting to varying numbers of classes and shots, for example).

The specific technical contributions of the paper and its organization are as follows. We start by introducing a probabilistic discriminative model for few-shot learning (see Section 2). This contrasts with recent work that has employed probabilistic generative models (Edwards and Storkey, 2017; Rezende et al., 2016), but discriminative models typically outperform their generative counterparts when predicting outputs from novel inputs (Ng and Jordan, 2002; Minka, 2005). The first contribution of the paper is to provide a framework for meta-learning probabilistic inference based upon a synthesis of Bayesian decision theory and amortization (see Section 2.2). The new framework is simple to implement, recovers state-of-the-art methods as special cases (Finn et al., 2017; Snell et al., 2017; Qiao et al., 2017; Ravi and Larochelle, 2017) (see Section 3), and suggests many generalizations. The second contribution of the paper is a highly flexible amortization network that takes few-shot learning datasets as inputs, with arbitrary numbers of classes and shots, and returns a trained neural network in a single forward pass per class (see Section 2.3). This is achieved by combining permutation invariant instance pooling (Zaheer et al., 2017) with context independent inference (Qiao et al., 2017). The two technical innovations yield the VERSA algorithm which is evaluated on three datasets in Section 4. On Omniglot and *mini*ImageNet the method sets new state-of-the-art results for one-shot learning, and can directly generalize to classification problems with large numbers of classes. The generality and power of the framework is then demonstrated through a challenging one-shot ShapeNet view reconstruction task.

2. Versatile Learning via Meta-Learned Amortized Bayesian Inference

We now present our framework that consists of (i) a probabilistic model, (ii) a framework for meta-learning probabilistic inference, and (iii) a versatile amortization scheme.

2.1. Probabilistic Model

Two principles guide the choice of model. First, the use of discriminative models to maximize predictive performance on supervised learning tasks (Ng and Jordan, 2002; Minka, 2005). Second, the need to leverage shared statistical structure between tasks (i.e. multi-task learning). These criteria are met by the directed graphical model shown in Fig. 1 that employs shared parameters θ and task specific parameters $\{\psi^{(t)}\}_{t=1}^T$. Inputs are denoted x and outputs y . Training data $D^{(t)} = \{(x_n^{(t)}, y_n^{(t)})\}_{n=1}^{N_t}$, and test data $\{(\tilde{x}_m^{(t)}, \tilde{y}_m^{(t)})\}_{m=1}^{M_t}$ are explicitly distinguished for each task t , as this is key for few-shot learning.

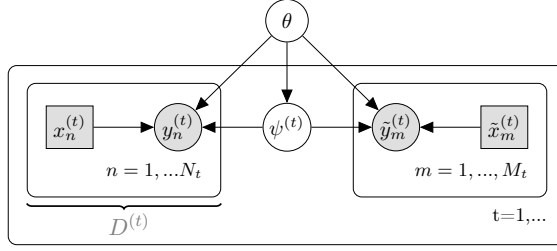


Figure 1: Directed graphical model for multi-task learning.

Let $X^{(t)}$ and $Y^{(t)}$ denote all the inputs and outputs (both test and train) for task t . The joint probability of the outputs and task specific parameters for T tasks, given the inputs and global parameters is:

$$p\left(\{Y^{(t)}, \psi^{(t)}\}_{t=1}^T | \{X^{(t)}\}_{t=1}^T, \theta\right) = \prod_{t=1}^T p\left(\psi^{(t)} | \theta\right) \prod_{n=1}^{N_t} p\left(y_n | x_n^{(t)}, \psi^{(t)}, \theta\right) \prod_{m=1}^{M_t} p\left(\tilde{y}_m | \tilde{x}_m^{(t)}, \psi^{(t)}, \theta\right).$$

For few-shot image classification, our parameterization of the probabilistic model is inspired by early work from Bakker and Heskes (2003) and recent extensions to deep learning (Bauer et al., 2017; Qiao et al., 2017). A feature extractor neural network $h_\theta(x) \in \mathbb{R}^{d_\theta}$, shared across all tasks, feeds into a set of task-specific linear classifiers with softmax outputs and weights and biases $\psi^{(t)} = \{W^{(t)}, b^{(t)}\}$ (see Fig. 2, *top left*). Learning will now be framed as a novel form of inference for θ and $\{\psi^{(t)}\}_{t=1}^T$ that supports meta-learning.

2.2. Bayesian Decision Theoretic Based Variational Training

The new inference framework is based upon Bayesian decision theory (BDT). BDT provides a recipe for making predictions \hat{y} for an unknown test variable \tilde{y} by combining information from observed training data $D^{(t)}$ (here from a single task t) and a loss function $L(\tilde{y}, \hat{y})$ that encodes the cost of predicting \hat{y} when the true value is \tilde{y} (Berger, 2013; Jaynes, 2003). In BDT an optimal prediction minimizes the expected loss (suppressing dependencies on the inputs and θ to reduce notational clutter):¹

$$\hat{y}^* = \operatorname{argmin}_{\hat{y}} \int p(\tilde{y} | D^{(t)}) L(\tilde{y}, \hat{y}) d\tilde{y}, \quad \text{where} \quad p(\tilde{y} | D^{(t)}) = \int p(\tilde{y} | \psi^{(t)}) p(\psi^{(t)} | D^{(t)}) d\psi^{(t)} \quad (1)$$

is the Bayesian predictive distribution and $p(\psi^{(t)} | D^{(t)})$ the posterior distribution of $\psi^{(t)}$ given the training data from task t .

BDT separates test and training data and so is a natural lens through which to view recent episodic approaches to training that utilize many internal training/test splits (Vinyals et al., 2016). Based on this insight, what follows is a fairly dense derivation of an ultimately simple stochastic variational objective for meta-learning probabilistic inference that is rigorously grounded in Bayesian inference and decision theory.

Distributional BDT. We generalize BDT to cases where the goal is to return a full predictive *distribution* $q(\cdot)$ over the unknown test variable \tilde{y} rather than a point prediction. The quality of q is quantified through a distributional loss function $L(\tilde{y}, q(\cdot))$. Typically, if \tilde{y} (the true value of the underlying variable) falls in a low probability region of $q(\cdot)$ the loss will be high, and vice versa. The optimal predictive q^* is found by optimizing the expected distributional loss with q constrained to a distributional family \mathcal{Q} :

$$q^* = \operatorname{argmin}_{q \in \mathcal{Q}} \int p(\tilde{y} | D^{(t)}) L(\tilde{y}, q(\cdot)) d\tilde{y}. \quad (2)$$

¹For discrete outputs the integral may be replaced with a summation.

Amortized variational training. Here, we amortize q to form quick predictions at test time and learn parameters by minimizing average expected loss *over tasks*. Let ϕ be a set of shared variational parameters such that $q(\tilde{y}) = q_\phi(\tilde{y}|D)$ (or q_ϕ for shorthand). Now the approximate predictive distribution can take any training dataset $D^{(t)}$ as an argument and directly perform prediction of $\tilde{y}^{(t)}$. The optimal variational parameters are found by minimizing the expected distributional loss across tasks

$$\phi^* = \operatorname{argmin}_{\phi} \mathcal{L}[q_\phi], \quad \mathcal{L}[q_\phi] = \int p(D) p(\tilde{y}|D) L(\tilde{y}, q_\phi(\cdot|D)) d\tilde{y} dD = \mathbb{E}_{p(D, \tilde{y})} [L(\tilde{y}, q_\phi(\cdot|D))]. \quad (3)$$

Here the variables D, \tilde{x} and \tilde{y} are placeholders for integration over all possible datasets, test inputs and outputs. Note that Eq. (3) can be stochastically approximated by sampling a task t and randomly partitioning into training data D and test data $\{\tilde{x}_m, \tilde{y}_m\}_{m=1}^M$, which naturally recovers episodic mini-batch training over tasks and data (Vinyals et al., 2016; Ravi and Larochelle, 2017). Critically, this does not require computation of the true predictive distribution. It also emphasizes the meta-learning aspect of the procedure, as the model is *learning how to infer* predictive distributions from training tasks.

Loss functions. We employ the log-loss: the negative log density of q_ϕ at \tilde{y} . In this case,

$$\mathcal{L}[q_\phi] = \mathbb{E}_{p(D, \tilde{y})} [-\log q_\phi(\tilde{y}|D)] = \mathbb{E}_{p(D)} [\text{KL}[p(\tilde{y}|D)||q_\phi(\tilde{y}|D)] + \text{H}[p(\tilde{y}|D)]], \quad (4)$$

where $\text{KL}[p(y)||q(y)]$ is the KL-divergence, and $\text{H}[p(y)]$ is the entropy of p . Eq. (4) has the elegant property that the optimal q_ϕ is the closest member of \mathcal{Q} (in a KL sense) to the true predictive $p(\tilde{y}|D)$, which is unsurprising as the log-loss is a proper scoring rule (Huszar, 2013). This is reminiscent of the sleep phase in the wake-sleep algorithm (Hinton et al., 1995). Exploration of alternative proper scoring rules (Dawid, 2007) and more task-specific losses (Lacoste-Julien et al., 2011) is left for future work.

Specification of the approximate predictive distribution. Next, we consider the form of q_ϕ . Motivated by the optimal predictive distribution, we replace the true posterior by an approximation:

$$q_\phi(\tilde{y}|D) = \int p(\tilde{y}|\psi) q_\phi(\psi|D) d\psi. \quad (5)$$

BDT meta-learning framework. Combining Eqs. (3) to (5) and re-introducing inputs yields:

$$\mathcal{L}(\phi) = -\mathbb{E}_{p(D, \tilde{y}, \tilde{x})} \left[\log \int p(\tilde{y}|\tilde{x}, \psi) q_\phi(\psi|D) d\psi \right], \quad (6)$$

which defines our inference framework. The procedure returns parameters that best approximate the Bayesian predictive distribution in an average KL sense. So, if the approximate posterior $q_\phi(\psi|D)$ is rich enough, optimization will recover the true posterior $p(\psi|D)$ (assuming $p(\psi|D)$ obeys identifiability conditions (Casella and Berger, 2002)).² Thus, the amortized BDT procedure meta-learns approximate inference.

End-to-end stochastic training. We also optimize over θ to maximize performance on the test tasks. Thus, an end-to-end stochastic training objective for θ and ϕ is:

$$\hat{\mathcal{L}}(\theta, \phi) = \frac{1}{MT} \sum_{M, T} \log \frac{1}{L} \sum_{l=1}^L p\left(\tilde{y}_m^{(t)} | \tilde{x}_m^{(t)}, \psi_l^{(t)}, \theta\right), \quad \text{with } \psi_l^{(t)} \sim q_\phi(\psi|D^{(t)}, \theta) \quad (7)$$

²Note that the true *predictive* posterior $p(y|D)$ is recovered regardless of the identifiability of $p(\psi|D)$.

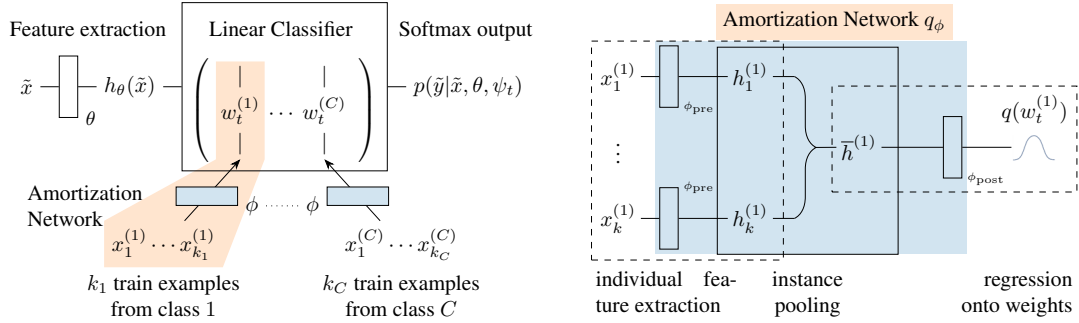


Figure 2: Computational flow of VERSA for few-shot classification with context-independent approximation. *Left:* A test point \tilde{x} is mapped to its softmax output through a feature extractor neural network and a linear classifier (fully connected layer). The global parameters θ of the feature extractor are shared between tasks whereas the weight vectors $w_t^{(c)}$ of the linear classifier are task specific and inferred through an amortization network with parameters ϕ . *Right:* Amortization network that maps k training examples of a particular class to the corresponding weight vector of the linear classifier.

and $\{\tilde{y}_m^{(t)}, \tilde{x}_m^{(t)}, D^{(t)}\} \sim \hat{p}(\tilde{y}, \tilde{x}, D)$, where \hat{p} represents the data distribution (e.g., sampling tasks and splitting them into training data D and test data $\{(\tilde{x}_m, \tilde{y}_m)\}_{m=1}^{M_t}$). This approximates the integral over ψ by Monte Carlo sampling with reparametrization (in practice we use local reparametrization (Kingma et al., 2015)) using L samples in addition to stochastic approximation. Notice that in Eqs. (6) and (7), q_ϕ depends only on the training data D , and not on the test data. Interestingly, the learning objective does not require an explicit specification of the prior distribution over parameters, $p(\psi_t|\theta)$, learning it implicitly through q_ϕ instead.

In summary, we have developed a Bayesian decision theoretic approach for meta-learning approximate inference tailored for prediction. Next, we discuss design choices that lead to the VERSA algorithm.

2.3. Versatile Amortized Inference

A versatile system is one that makes inferences both rapidly *and* flexibly. By rapidly we mean that test-time inference involves only simple computation such as a feed-forward pass through a neural network. By flexibly we mean that the system supports a variety of tasks – including variable numbers of classes, and sizes of training / testing sets – without retraining. Rapid inference comes automatically with the use of a deep neural network to amortize the approximate posterior distribution q . However, it comes at the cost of flexibility: amortized inference is typically limited to a single specific task. Below, we discuss design choices that enable us to retain flexibility.

Inference with sets as inputs. The amortization network takes data sets of variable size as inputs whose ordering we should be invariant to. We therefore use permutation-invariant *instance-pooling* operations to process these sets of points similarly to Qi et al. (2017) and as formalized in Zaheer et al. (2017). The instance-pooling operation ensures that the network can process any number of training observations. When a distributional q is employed, it is important to choose a pooling operation that is *not* scale invariant (e.g., sum rather than mean), to provide information regarding the number of training examples available, which is critical for modeling uncertainty.

Context independent inference. In the few-shot classification setting, a naive amortization requires the approximate posterior $q_\phi(\psi|D, \theta)$ to model the distribution over full weight matrices in $\mathbb{R}^{d_\theta \times C}$ (and biases). This requires the specification of the number of few-shot classes C ahead of time and limits inference to this chosen number. Moreover, it is difficult to meta-learn systems that

directly output large matrices as the output dimensionality is high and it is unclear how to share information between tasks. We therefore propose specifying $q_\phi(\psi|D, \theta)$ in a *context independent* manner such that each weight vector ψ_c depends only on examples from class c , by amortizing individual weight vectors associated with a single softmax output instead of the entire weight matrix directly:

$$q_\phi(\psi|D, \theta) = \prod_{c=1}^C q_\phi\left(\psi_c|\{x_n^c\}_{n=1}^{k_c}, \theta\right). \quad (8)$$

Here k_c is the number of observed examples $\{x_n^c\}_{n=1}^{k_c}$ in class c and $\psi_c = \{w_c, b_c\}$ denotes the weight vector and bias of the linear classifier associated with that class. Thus, we construct the classification matrix $\psi^{(t)}$ by performing C feed-forward passes through the inference network q_ϕ (see Fig. 2 *left*). Note that to reduce the number of learned parameters, it is possible to share parts of θ and ϕ , e.g., by using the last hidden layer as input to the amortization network.

The assumption of context independent inference is an approximation. In Appendix B, we provide empirical justification for its validity. Full approximate posterior distributions are shown to be close to context independent. Critically, the context independent approximation addresses all the limitations of a naive amortization mentioned above: (i) the inference network needs to amortize far fewer parameters whose number does not scale with number of classes C (a single weight vector instead of the entire matrix); (ii) it is clear how meta-learning can share information between tasks; (iii) the number of classes C can vary at inference time.

Point parameter estimates. We use deterministic parameter estimates $q_\phi(\psi|D, \theta) = \delta(\psi - \psi_\phi^*(D, \theta))$ for two reasons. First, in Section 3 we show that many existing approaches to few-shot learning are encompassed by this special case with different choices for the local parameter point-estimates $\psi_\phi^*(D, \theta)$ (e.g., Finn et al. (2017); Snell et al. (2017); Qiao et al. (2017); Ravi and Larochelle (2017)). Second, experiments indicate that although distributional versions can recover more accurate uncertainty estimates, prediction error is not adversely affected by employing point estimates (see Appendices A and C). Thus, to maintain simplicity and speed, VERSA employs point estimates and Eq. (7) reduces to:

$$\theta^*, \phi^* = \operatorname{argmax}_{\theta, \phi} \frac{1}{MT} \sum_{M, T} \log p\left(\tilde{y}_m^{(t)}|\tilde{x}_m^{(t)}, \psi_\phi^*(D^{(t)}, \theta), \theta\right), \quad \{\tilde{y}_m^{(t)}, \tilde{x}_m^{(t)}, D^{(t)}\} \sim \hat{p}(\tilde{y}, \tilde{x}, D). \quad (9)$$

3. Related Work

A number of recent approaches to few-shot and meta-learning can be cast as instances of the BDT meta-learning framework employing $q(\psi^{(t)}|D^{(t)}, \theta) = \delta(\psi^{(t)} - \psi^*(D^{(t)}, \theta))$. Here we explore these connections and compare them to VERSA.

Gradient-Based Meta-Learning. Much of the recent focus on meta-learning has framed gradient-based optimization as a key ingredient. Ravi and Larochelle (2017) proposed training a recurrent neural network (RNN) to learn how to perform a few gradient steps to optimize model performance on a new dataset. Finn et al. (2017) proposed learning a global initialization that can be optimized with a small number of gradient steps based on a few examples from a new task. We now show how those works can be cast as instances of the VERSA framework by specific choices for $\psi^*(D^{(t)}, \theta)$.

Let the local parameters $\psi^{(t)}$ and the estimate $\psi^*(D^{(t)}, \theta)$ be:

$$\psi^{(t)} = \text{all neural network parameters}; \quad \psi^*(D^{(t)}, \theta) = \psi_0 + \eta \frac{\partial}{\partial \psi} \log \sum_{n=1}^{N_t} p(y_n^{(t)}|x_n^{(t)}, \psi, \theta) \Big|_{\psi_0}. \quad (10)$$

Here ψ^* is given by taking a step of gradient ascent of the training loss, initialized at ψ_0 and with learning rate η . This is semi-amortized inference (Kim et al., 2018), as the only shared

inference parameters are the initialization and learning rate, and optimization is required for each task. Importantly, Eq. (10) recovers *Model-agnostic meta-learning* (Finn et al., 2017), providing a perspective as semi-amortized Bayesian decision theory which is complementary to existing probabilistic interpretations (Grant et al., 2018). Ravi and Larochelle (2017) can be viewed as a generalization to multiple gradient steps where an RNN computes ψ^* . By comparison to these methods, VERSA relieves the need to back-propagate through gradient based procedures during training, fully-amortizes the cost of inference at test time, and enables the treatment of both local and global parameters which helps simplify inference.

Metric-Based Few-Shot Learning. Snell et al. (2017) recently proposed *prototypical networks*, a method that achieves excellent performance in a number of few-shot learning tasks. Prototypical networks are based on the idea that an embedding (represented by a neural network h_θ) may be learned such that examples from a class c will cluster around a prototype μ_c in the embedded space. Given such an embedding, nearest-neighbour based classification (with a specified distance function d) can achieve high classification accuracy.

We can recover prototypical networks in our framework by letting the local parameters $\psi^{(t)}$ and the estimate $\psi^*(D^{(t)}, \theta)$ be:

$$\psi^{(t)} = \{w_c^{(t)}, b_c^{(t)}\}_{c=1}^C, \quad \psi^*(D^{(t)}, \theta) = \{w_c^*, b_c^*\}_{c=1}^C = \left\{ \mu_c^{(t)}, -\frac{\|\mu_c^{(t)}\|^2}{2} \right\}_{c=1}^C$$

where $\mu_c^{(t)} = \frac{1}{k_c} \sum_{n=1}^{k_c} h_\theta(x_n^{(c)})$ are the means of the feature representation of the inputs from class c for task t . These choices lead to the following predictive distribution:

$$p(y = c|x, \theta) \propto \exp(-d(h_\theta(x), \mu_c)) = \exp\left(h_\theta(x)^T \mu_c - \frac{1}{2}\|\mu_c\|^2\right),$$

which recovers prototypical networks using a Euclidean distance function d . In comparison, VERSA is more general in that it introduces a more flexible parametric form for q that enables meta-learning of the predictive distribution, and can be extended to account for predictive uncertainty.

Inferring Weights from Activations. Qiao et al. (2017) recently proposed a method for predicting weights of classes from activations of a pre-trained network to support: i) online learning on a single task to which new few-shot classes are incrementally added; and ii) transferring from a high-shot classification task to a separate low-shot classification task. VERSA’s amortization network is similar in spirit, but it is more general at training and test time: it employs end-to-end training, supports full multi-task learning, shares information between many tasks, and is flexible at test time.

Variational Inference (VI). Standard application of amortized VI (Kingma and Welling, 2014; Rezende et al., 2014; Kingma et al., 2015; Blundell et al., 2015) for ψ in the multi-task discriminative model optimizes the Monte Carlo approximated free-energy w.r.t. ϕ and θ :

$$\hat{\mathcal{L}}(\theta, \phi) = \frac{1}{T} \sum_{t=1}^T \left(\sum_{(x,y) \in D^{(t)}} \left(\frac{1}{L} \sum_{l=1}^L \log p(y|x, \psi_l^{(t)}, \theta) \right) - \text{KL} \left[q_\phi(\psi|D^{(t)}, \theta) \| p(\psi|\theta) \right] \right), \quad (11)$$

where $\psi_l^{(t)} \sim q_\phi(\psi|D^{(t)}, \theta)$. On one hand, when the approximate posterior becomes a delta-function (meaning that the KL can be dropped) VI is similar to the VERSA training objective in Eq. (9). However, since VI does not employ internal test-train splits at training time, such variants can suffer from over-fitting. On the other hand, if a distributional approximate posterior is retained instead, VI tends to under-fit (Trippe and Turner, 2018) also adversely affecting performance. In contrast Appendix C shows that VERSA *significantly outperforms* VI in the few-shot classification case, and that retaining a full distributional posterior does not negatively affect accuracy.

4. Experiments and Results

We evaluate VERSA on a set of few-shot learning tasks. We report few-shot classification results using the Omniglot and *miniImageNet* datasets in Section 4.1, and demonstrate VERSA’s ability to retain high accuracy as the shot and way is varied at test time. In Section 4.2, we examine VERSA’s performance on a one-shot view reconstruction task with ShapeNet objects.³

4.1. Few-shot Classification

We evaluate VERSA on standard few-shot classification tasks in comparison to previous work. Experimentation consists of evaluating models in learning of C -way classification tasks with k_c examples per class using the Omniglot (Lake et al., 2011) and *miniImageNet* (Ravi and Larochelle, 2017) datasets. VERSA follows the implementation in Section 2, and the approximate inference scheme in Eq. (8). We follow the experimental protocol established by Vinyals et al. (2016) for Omniglot and Ravi and Larochelle (2017) for *miniImageNet*, using equivalent architectures for h_θ . Training is carried out in an episodic manner: for each task, k_c examples are used as training inputs to infer $q_\phi(\psi_c|D, \theta)$ for each class, and an additional set of examples is used to evaluate the objective function.

Omniglot training procedure. Omniglot is a few-shot learning dataset consisting of 1623 hand-written characters (each with 20 instances) derived from 50 alphabets. We follow a pre-processing and training procedure akin to that defined in (Vinyals et al., 2016). First the images are resized to 28×28 pixels and then character classes are augmented with rotations of 90 degrees. The training, validation and test sets consist of a random split of 1100, 100, and 423 characters, respectively. When augmented this results in 4400 training, 400 validation, and 1292 test classes, each having 20 character instances. For C -way, k_c -shot classification, training proceeds in an episodic manner. Each training iteration consists of a batch of one or more tasks. For each task C classes are selected at random from the training set. For each training class, k_c character instances are used as training inputs and the remaining $(20 - k_c)$ character instances are used as test inputs. The validation set is used to monitor the progress of learning and to select the best model to test, but does not affect the training process. Testing is done on 600 randomly selected tasks from the test set. We use the Adam (Kingma and Ba, 2015) optimizer with a constant learning rate of 0.0001 for 60,000 iterations with 16 tasks per batch to train all models. In addition, we set $d_\theta = 256$ and number of ψ samples to $L = 1$. However given that we set $q(\psi|D, \theta) = \delta(\psi - \psi^*(D, \theta))$, the value of L makes no difference.

miniImageNET training procedure. *miniImageNet* is a dataset of 60,000 color images that is sub-divided into 100 classes, each with 600 instances. The images have dimensions of 84×84 pixels. For our experiments, we use the 64 training, 16 validation, and 20 test class splits defined by (Ravi and Larochelle, 2017). Training proceeds in the same episodic manner as with Omniglot with the exception that we always use 15 instances as test inputs. We use the Adam (Kingma and Ba, 2015) optimizer, train for 50,000 iterations, set $d_\theta = 256$, and number of ψ samples to $L = 1$. For the 1-shot model, we train with 8 tasks per batch and use a constant learning rate of 0.00025. For the 5-shot model, we train using 4 tasks per batch and use a constant learning rate of 0.0001.

Refer to Appendix D.1 for complete details on the VERSA network architectures used in the few-shot classification experiments.

Results. Table 1 details few-shot classification performance on both datasets for VERSA as well as competitive approaches. Note that the training, validation, and test splits have not been specified for previous methods, affecting the comparison. For both datasets, VERSA achieves state

³Source code accompanying the paper will be made available.

Method	<i>Omniglot</i>				<i>miniImageNet</i>				
	5-way accuracy		20-way accuracy		5-way accuracy				
	■ 1-shot	● 5-shot	■ 1-shot	● 5-shot	■ 1-shot	● 5-shot	● 5-shot		
	98	99	100	90	95	100	50	60	70
Matching (Vinyals et al., 2016)	■	●			■	●	■	●	
Meta LSTM (Ravi and Larochelle, 2017)							■	●	●
Neural Stat (Edwards and Storkey, 2017)	■		●		■	●			
memory mod (Kaiser et al., 2017)	■		●		■	●			
Prototypical (Snell et al., 2017)		■	●		■	●	■		●
MAML (Finn et al., 2017)		■	●		■	●	■	●	●
Reptile (Nichol and Schulman, 2018)	■		●		■	●	■		●
VERSA		■	●			■	■	●	●

Table 1: Results and comparison for 1-shot (■) and 5-shot (●) image classification on Omniglot and *miniImageNet*. Error bars indicate the 95% confidence interval over tasks using a Student’s t-distribution approximation. For numerical values see Tables D.4 and D.5.

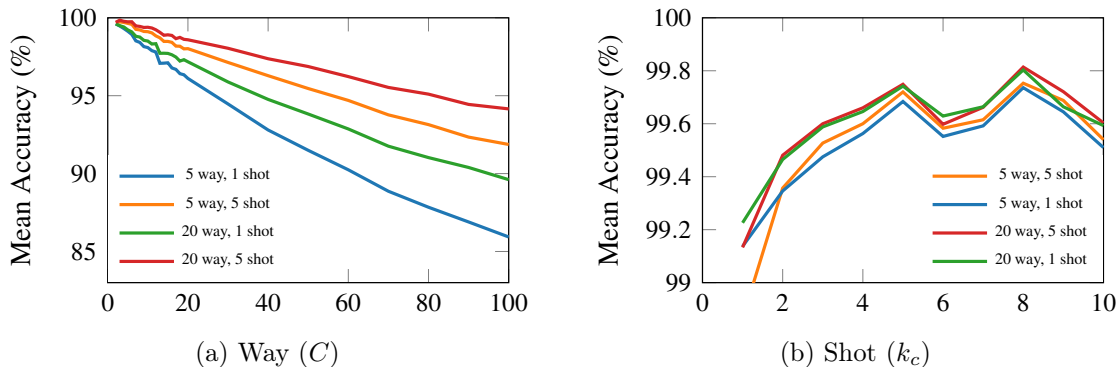


Figure 3: Test accuracy on Omniglot when varying (a) way (fixing shot to be that used for training) and (b) shot. In Fig. 3b, all models are evaluated on 5-way classification. Colors indicate models trained with different way-shot episodic combinations.

of the art results on 1-shot learning: 99.24% (up 0.44%) and 97.24% (up 1.24%) for Omniglot 5- and 20-way respectively, and 50.70% (up 0.73%) for 5-way *miniImageNet*. For Omniglot 5-shot learning, VERSA’s performance is within error bars of state of the art. For *miniImageNet* 5-shot learning, VERSA improves on most approaches with the exception of the work of Snell et al. (2017) (down 3.17%), who train their model on significantly higher C -way tasks than test-performance is evaluated on.

VERSA allows us to vary the number of classes C and shots k_c between training and testing (Eq. (8)). Fig. 3a shows that a model trained for a particular C -way retains very high accuracy as C is varied. Even for $C = 100$, the 20-Way, 5-Shot VERSA has an accuracy of approximately 94%. Fig. 3b shows a similarly robust result as k_c is varied. This unique aspect of VERSA demonstrates considerable flexibility in that a trained model is robust when additional classes or fewer shots are presented at test time. This adaptability enables efficiencies as it requires only forward passes through the network.

4.2. ShapeNet View Reconstruction

To demonstrate the generality of the framework we consider a challenging few-shot learning task with a complex output space. We define view recovery as the ability to infer how an object looks from any desired angle based on a small set of observed views. We frame this as a multi-output regression task from a set of training images with known orientations to output images with specified orientations.

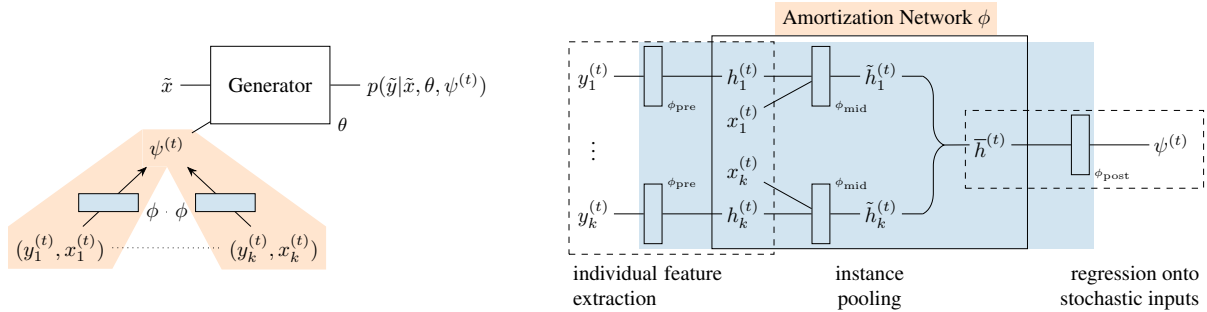


Figure 4: Computational flow of VERSA for few-shot view recovery. *Left*: A set of training images and angles $\{(y_n^{(t)}, x_n^{(t)})\}_{n=1}^k$ are mapped to a stochastic input $\psi^{(t)}$ through the amortization network q_ϕ . $\psi^{(t)}$ is then concatenated with a test angle \tilde{x} and mapped onto a new image through the generator θ . *Right*: Amortization network that maps k image/angle examples of a particular object-instance to the corresponding stochastic input.

We let θ be the parameters of a neural network that acts as a generator for images, and specify $\psi^{(t)}$ to be an *object-instance level* stochastic input to the generator. ϕ parameterizes a network that first processes the image representations of an object, then concatenates them with their associated view orientations, processes them further before instance-pooling, from which q_ϕ produces a distribution over $\psi^{(t)}$. We set $q(\psi|D, \theta) = \delta(\psi - \psi^*(D, \theta))$ (see Fig. 4).

View reconstruction training procedure. ShapeNetCore v2 (Chang et al., 2015) is an annotated database of 3D objects covering 55 common object categories with 51,300 unique objects. For our experiments, we use only 2 of the largest object categories: airplanes (synset ID 02691156 with 4045 instances) and chairs (synset ID 03001627 with 6778 instances). For each object set, we use 70% of the objects for training, 10% for validation, and 20% for testing. For each object, we generate $V = 36$, 128×128 pixel image views spaced evenly every 10 degrees in azimuth around the object. We then convert the rendered images to gray-scale and reduce their size to be 32×32 pixels. Again, we train our model in an episodic manner. Each training iteration consists a batch of one or more tasks. For each task an object is selected at random from the training set. We train on a single view selected at random from the $V = 36$ views associated with each object and use the remaining 35 views to evaluate the objective function. We then generate 36 views of the object with a modified version of our amortization network which is shown diagrammatically in Fig. 4. To train, we use the Adam (Kingma and Ba, 2015) optimizer with a constant learning rate of 0.0001 with 8 tasks per batch for 150,000 training iterations for the planes model and 200,000 iterations for the chairs model. In addition, we set $d_\phi = 256$, $d_\psi = 256$ and number of ψ samples to 1.

Results. We evaluate VERSA by comparing it to a conditional variational autoencoder (C-VAE) with view angles as labels (Kingma et al., 2014; Narayanaswamy et al., 2017) and identical architectures, using a subset of the ShapeNetCore v2 database of 3D objects. While VERSA is trained in an episodic manner, the C-VAE is trained in batch-mode. We train on a single view selected at random and use the remaining views to evaluate the objective function. Fig. 5 shows images of unseen planes and chairs generated from a single shot with VERSA as well as a C-VAE and compares both to ground truth images. Table 2 provides quantitative comparison results between VERSA and the C-VAE. Both VERSA and the C-VAE capture the correct orientation of the object in the generated images. However, VERSA produces images that contain much more detail and are visually sharper than the C-VAE images. The quantitative metrics all show the superiority of VERSA over a C-VAE (see Table 2).

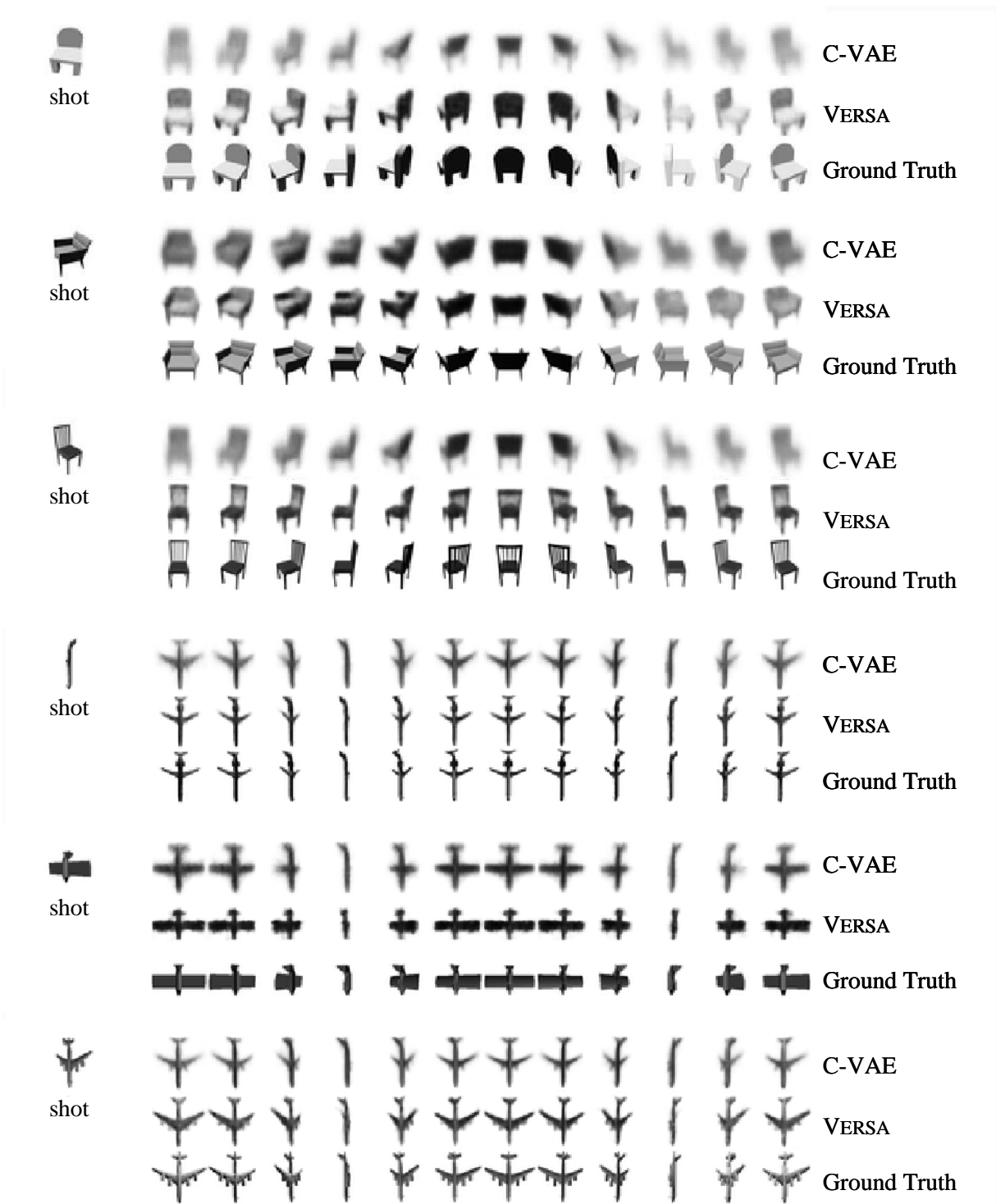


Figure 5: Results for ShapeNet view reconstruction for unseen chairs and planes from the test set (shown left). Models were trained to reconstruct views from a single orientation. *Top row*: images/views generated by a C-VAE model; *middle row* images/views generated by VERSA; *bottom row*: ground truth images. Views are spaced evenly every 30 degrees in azimuth.

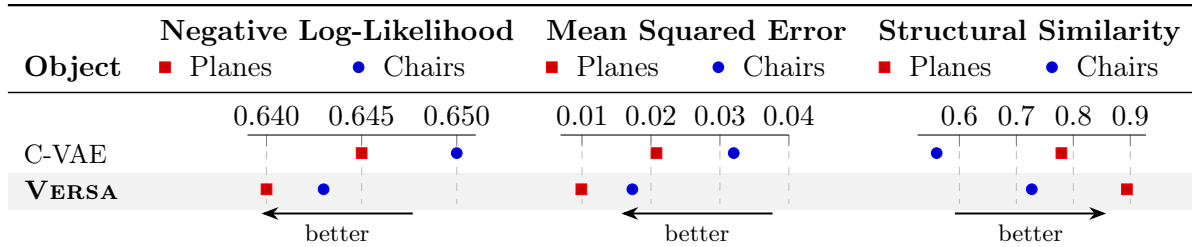


Table 2: ShapeNet view reconstruction test results. Negative log-likelihood is measured in bits per pixel. Mean squared error and structural similarity index are measured between generated and ground truth images. Averages are taken over 100 randomly selected objects from the test set where 36 images uniformly spaced in azimuth are generated from a single shot.

5. Conclusions

We introduced a new probabilistic deep learning framework consisting of three key ingredients: (i) discriminative probabilistic modeling that leverages shared information across related supervised tasks; (ii) a novel, Bayesian decision theoretic approach to meta-learning probabilistic inference across many tasks; and (iii) fast and flexible amortization of inference for task-specific variables. Put together, this yields a simple to implement, flexible, and scalable framework for data efficient and versatile deep learning. We introduced **VERSA**, a versatile deep learning algorithm, that achieves state-of-the-art performance on one-shot classification tasks. **VERSA** exhibited versatility and robustness by retaining high accuracy as the number of classes are significantly increased and few-shot examples are decreased at test time. Moreover, we showed quantitative and qualitative results in a challenging one-shot view recovery task for 3D objects from the ShapeNet dataset. We believe that there are significant potential benefits in further exploring the use of BDT for meta-learning tasks.

Acknowledgements

We thank Ravi and Larochelle for providing the *miniImageNet* dataset. M.B. acknowledges partial funding by the EPSRC and a Qualcomm European Scholarship in Technology. R.E.T. acknowledges support from EPSRC grants EP/M0269571 and EP/L000776/1. J.G. acknowledges funding from a Samsung Doctoral Scholarship.

References

- B. Bakker and T. Heskes. Task clustering and gating for Bayesian multitask learning. *Journal of Machine Learning Research*, 4(May):83–99, 2003.
- M. Bauer, M. Rojas-Carulla, J. B. Świątkowski, B. Schölkopf, and R. E. Turner. Discriminative k-shot learning using probabilistic models. *arXiv preprint arXiv:1706.00326*, 2017.
- J. O. Berger. *Statistical decision theory and Bayesian analysis*. Springer Science & Business Media, 2013.
- C. Blundell, J. Cornebise, K. Kavukcuoglu, and D. Wierstra. Weight uncertainty in neural network. In *International Conference on Machine Learning*, pages 1613–1622, 2015.
- G. Casella and R. L. Berger. *Statistical inference*, volume 2. Duxbury Pacific Grove, CA, 2002.
- A. X. Chang, T. Funkhouser, L. Guibas, P. Hanrahan, Q. Huang, Z. Li, S. Savarese, M. Savva, S. Song, H. Su, J. Xiao, L. Yi, and F. Yu. ShapeNet: An Information-Rich 3D Model Repository. Technical Report arXiv:1512.03012 [cs.GR], Stanford University — Princeton University — Toyota Technological Institute at Chicago, 2015.
- A. P. Dawid. The geometry of proper scoring rules. *Annals of the Institute of Statistical Mathematics*, 59(1):77–93, 2007.
- H. Edwards and A. Storkey. Towards a neural statistician. In *Proceedings of the International Conference on Learning Representations (ICLR)*, 2017.
- C. Finn, P. Abbeel, and S. Levine. Model-agnostic meta-learning for fast adaptation of deep networks. In *International Conference on Machine Learning*, pages 1126–1135, 2017.
- E. Grant, C. Finn, S. Levine, T. Darrell, and T. Griffiths. Recasting gradient-based meta-learning as hierarchical Bayes. In *Proceedings of the International Conference on Learning Representations (ICLR)*, 2018.
- G. E. Hinton, P. Dayan, B. J. Frey, and R. M. Neal. The "wake-sleep" algorithm for unsupervised neural networks. *Science*, 268(5214):1158–1161, 1995.
- F. Huszar. *Scoring rules, divergences and information in Bayesian machine learning*. PhD thesis, University of Cambridge, 2013.
- E. T. Jaynes. *Probability theory: the logic of science*. Cambridge university press, 2003.
- L. Kaiser, O. Nachum, R. Aurko, and S. Bengio. Learning to remember rare events. In *International Conference on Learning Representations (ICLR)*, 2017.
- Y. Kim, S. Wiseman, A. C. Miller, D. Sontag, and A. M. Rush. Semi-amortized variational autoencoders. In *Proceedings of the 35th International Conference on Machine Learning*, 2018.
- D. Kingma and J. Ba. Adam: A method for stochastic optimization. In *Proceedings of the International Conference on Learning Representations (ICLR)*, 2015.
- D. P. Kingma and M. Welling. Auto-encoding variational Bayes. In *Proceedings of the International Conference on Learning Representations (ICLR)*, 2014.
- D. P. Kingma, S. Mohamed, D. J. Rezende, and M. Welling. Semi-supervised learning with deep generative models. In *Advances in Neural Information Processing Systems*, pages 3581–3589, 2014.

- D. P. Kingma, T. Salimans, and M. Welling. Variational dropout and the local reparameterization trick. In *Advances in Neural Information Processing Systems*, pages 2575–2583, 2015.
- G. Koch, R. Zemel, and R. Salakhutdinov. Siamese neural networks for one-shot image recognition. In *ICML Deep Learning Workshop*, volume 2, 2015.
- S. Lacoste-Julien, F. Huszár, and Z. Ghahramani. Approximate inference for the loss-calibrated Bayesian. In *Proceedings of the Fourteenth International Conference on Artificial Intelligence and Statistics*, pages 416–424, 2011.
- B. Lake, R. Salakhutdinov, J. Gross, and J. Tenenbaum. One shot learning of simple visual concepts. In *Proceedings of the Annual Meeting of the Cognitive Science Society*, volume 33, 2011.
- L. v. d. Maaten and G. Hinton. Visualizing data using t-SNE. *Journal of machine learning research*, 9(Nov):2579–2605, 2008.
- T. Minka. Discriminative models, not discriminative training. Technical report, 2005.
- D. K. Naik and R. Mammone. Meta-neural networks that learn by learning. In *Neural Networks, 1992. IJCNN., International Joint Conference on*, volume 1, pages 437–442. IEEE, 1992.
- S. Narayanaswamy, T. B. Paige, J.-W. van de Meent, A. Desmaison, N. Goodman, P. Kohli, F. Wood, and P. Torr. Learning disentangled representations with semi-supervised deep generative models. In *Advances in Neural Information Processing Systems*, pages 5927–5937, 2017.
- A. Y. Ng and M. I. Jordan. On discriminative vs. generative classifiers: A comparison of logistic regression and naive bayes. In *Advances in Neural Information Processing Systems*, pages 841–848, 2002.
- A. Nichol and J. Schulman. Reptile: a scalable metalearning algorithm. *arXiv preprint arXiv:1803.02999*, 2018.
- C. R. Qi, H. Su, K. Mo, and L. J. Guibas. Pointnet: Deep learning on point sets for 3d classification and segmentation. *Proc. Computer Vision and Pattern Recognition (CVPR), IEEE*, 1(2):4, 2017.
- S. Qiao, C. Liu, W. Shen, and A. Yuille. Few-shot image recognition by predicting parameters from activations. *arXiv preprint arXiv:1706.03466*, 2017.
- S. Ravi and H. Larochelle. Optimization as a model for few-shot learning. In *Proceedings of the International Conference on Learning Representations (ICLR)*, 2017.
- D. Rezende, I. Danihelka, K. Gregor, D. Wierstra, et al. One-shot generalization in deep generative models. In *International Conference on Machine Learning*, pages 1521–1529, 2016.
- D. J. Rezende, S. Mohamed, and D. Wierstra. Stochastic backpropagation and approximate inference in deep generative models. In *International Conference on Machine Learning*, pages 1278–1286, 2014.
- J. Schmidhuber. *Evolutionary principles in self-referential learning*. PhD thesis, Technische Universität München, 1987.
- J. Snell, K. Swersky, and R. Zemel. Prototypical networks for few-shot learning. In *Advances in Neural Information Processing Systems*, pages 4080–4090, 2017.
- S. Thrun and L. Pratt. *Learning to learn*. Springer Science & Business Media, 2012.

- B. Trippe and R. Turner. Overpruning in variational bayesian neural networks. *arXiv preprint arXiv:1801.06230*, 2018.
- O. Vinyals, C. Blundell, T. Lillicrap, D. Wierstra, et al. Matching networks for one shot learning. In *Advances in Neural Information Processing Systems*, pages 3630–3638, 2016.
- M. J. Wainwright and M. I. Jordan. Graphical models, exponential families, and variational inference. *Foundations and Trends® in Machine Learning*, 1(1-2):1–305, 2008.
- Z. Wang, A. C. Bovik, H. R. Sheikh, and E. P. Simoncelli. Image quality assessment: from error visibility to structural similarity. *IEEE transactions on image processing*, 13(4):600–612, 2004.
- M. Zaheer, S. Kottur, S. Ravanbakhsh, B. Póczos, R. R. Salakhutdinov, and A. J. Smola. Deep sets. In *Advances in Neural Information Processing Systems*, pages 3394–3404, 2017.

A. Comparing Gaussian and δ -Function Forms of q

To investigate the properties of score function based approximation, we run the following experiment. We first generate data from the following generative process:

$$p(\theta) = \delta(\theta - 0), \quad (\text{A.1})$$

$$p(\psi|\theta) = \mathcal{N}(\psi; \theta, \sigma_\psi^2), \quad (\text{A.2})$$

$$p(y|\psi) = \mathcal{N}(y; \psi, \sigma_y^2). \quad (\text{A.3})$$

We generate $T = 250$ tasks from the above process, each having $N = 15$ train observations and $M = 25$ test observations. We then let $q_\phi(\psi|D^{(t)}) = \mathcal{N}(\psi; \mu_q^{(t)}, \sigma_q^{(t)2})$, amortizing inference as:

$$\mu_q^{(t)} = w_\mu \sum_{n=1}^N y_n^{(t)} + b_\mu, \quad \sigma_q^{(t)2} = \exp\left(w_\sigma \sum_{n=1}^N y_n^{(t)} + b_\sigma\right). \quad (\text{A.4})$$

The learnable parameters are thus $\phi = \{w_\mu, b_\mu, w_\sigma, b_\sigma\}$, and are trained with the following objective function:

$$\phi^* = \underset{\phi}{\operatorname{argmin}} \mathcal{L}[q_\phi] = \underset{\phi}{\operatorname{argmin}} \frac{1}{T} \frac{1}{M} \sum_{t=1}^T \sum_{m=1}^M L(y_m^{(t)}, q_\phi(\cdot|D^{(t)})), \quad (\text{A.5})$$

where $q_\phi(\cdot|D^{(t)}) = \int p(\cdot|\psi) q_\phi(\psi|D^{(t)}) d\psi$. Below, we discuss how to investigate the different forms of q (Gaussian and δ -function) by specifying forms of $L(y, q_\phi(\cdot|D^{(t)}))$.

A.1. Log of Expected Held-Out Likelihood (Gaussian q)

The loss function we focus on and experiment with is defined as:

$$L_1(y, q_\phi(\cdot|D^{(t)})) = -\log q_\phi(y|D^{(t)}) \quad (\text{A.6})$$

and corresponds to the log of expected (held-out) log-likelihood. As this choice is a proper scoring rule, it should therefore result in the optimal q being close to the true posterior predictive. Plugging this into Eq. (A.5), we have:

$$\mathcal{L}_1[q_\phi] = -\frac{1}{MT} \sum_{t=1}^T \sum_{m=1}^M \log \mathcal{N}(y_m^{(t)}; \mu_q^{(t)}, \sigma_q^{(t)2} + \sigma_y^2). \quad (\text{A.7})$$

A.2. Average Held-Out Log-Likelihood (δ -function q)

Here, we propose a slight manipulation to the loss function, such that:

$$L_2(y, q_\phi(\cdot|D^{(t)})) = -\int q_\phi(\psi|D^{(t)}) \log p(y|\psi) d\psi, \quad (\text{A.8})$$

and corresponds to average held-out log-likelihood. Plugging this into Eq. (A.5), we have:

$$\mathcal{L}_2[q_\phi] = \frac{1}{2MT} \sum_{t=1}^T \sum_{m=1}^M \left(\log 2\pi\sigma_y^2 + \frac{1}{\sigma_y^2} \left(y_m^{(t)2} + \mu_q^{(t)2} + \sigma_q^{(t)2} - 2y_m^{(t)}\mu_q^{(t)} \right) \right). \quad (\text{A.9})$$

Note that Eq. (A.9) monotonically decreases with σ_q^2 . Thus, this score function corresponds to setting $q_\phi(\psi|D) = \delta(\psi - \psi^*(D))$, as the optimization encourages $\sigma_q^2 \rightarrow 0$.

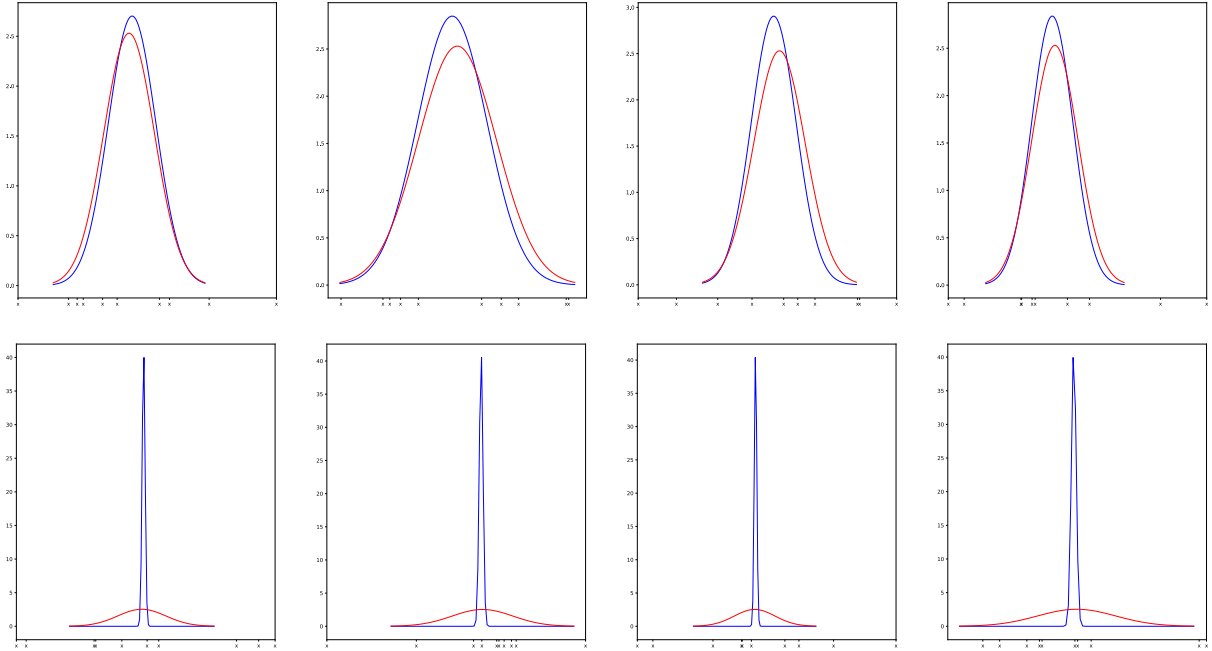


Figure A.1: Example true (red) and approximate (blue) posteriors for test sets in the experiment. (Top) Approximate posteriors generated by amortization network trained by optimizing $\bar{\mathcal{L}}_1$ and (bottom) approximate posteriors generated by amortization network trained by optimizing $\bar{\mathcal{L}}_2$.

A.3. Optimization and Results

Both objective functions are minimized using Adam (Kingma and Ba, 2015), using mini-batches of tasks from the generated dataset. The models are trained to convergence.⁴ Then, a separate set of tasks is generated from the same generative process, and the posterior $q_\phi(\psi|D)$ is inferred with the learned amortization parameters. Due to the simple generative process, the true posterior over ψ is Gaussian, and may be computed analytically.

Fig. A.1 show the approximate posterior distributions inferred for unseen test sets by amortization networks trained with (top) \mathcal{L}_1 and (bottom) \mathcal{L}_2 . This empirically strengthens the hypothesis that \mathcal{L}_1 is a sensible objective function for approximate inference, and that \mathcal{L}_2 converges on a point estimate approximation of this.

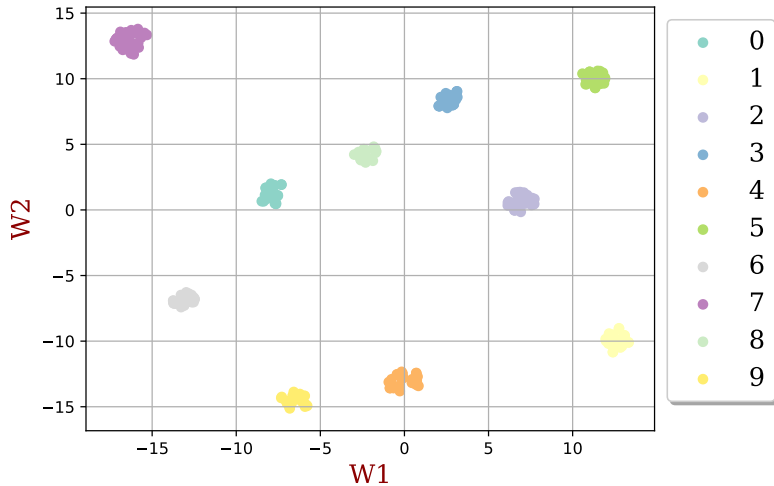
B. Empirical Justification for Context-Independent Approximation

Here we detail a simple experiment to evaluate the validity of the context-independent inference assumption. The goal of the experiment is to examine if weights may be context-independent without imposing the assumption on the amortization network. To see this, we randomly generate fifty tasks from a dataset, where classes may appear a number of times in different tasks. We then perform free-form (non-amortized) variational inference on the weights for each of the tasks, with a Gaussian variational distribution:

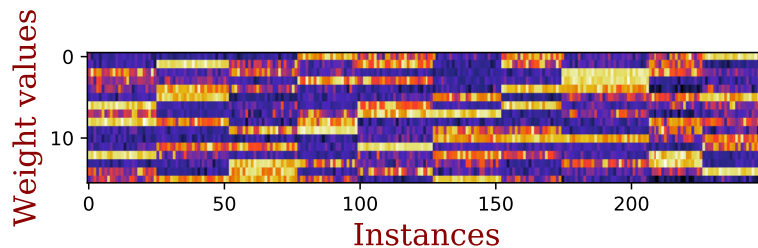
$$q_\phi \left(W^{(t)} | \mathcal{D}^{(t)}, \theta \right) = \mathcal{N} \left(W^{(t)}; \mu_\phi^{(t)}, \sigma_\phi^{(t)2} \right). \quad (\text{B.1})$$

If the assumption is reasonable, we may expect the distribution of the weights of a specific class to be similar regardless of the additional classes in the task.

⁴For $\bar{\mathcal{L}}_2$, early-stopping was employed during optimization to prevent the variance to grow too small (for visualization purposes).



(a)



(b)

Figure B.1: Visualizing the learned weights for $d_\theta = 16$. (a) Weight dimensionality is reduced using T-SNE (Maaten and Hinton, 2008). Weights are colored according to class. (b) Each weight represents one column of the image. Weights are grouped by class.

We examine 5-way classification in the MNIST dataset. We randomly sample and fix fifty such tasks. We train the model twice using the same feature extraction network used in the few-shot classification experiments, and fix the d_θ to be 16 and 2. We then train the model in an episodic manner by mini-batching tasks at each iteration. The model is trained to convergence, and achieves 99% accuracy on held out test examples for the tasks. After training is complete we examine the optimized $\mu_\phi^{(t)}$ for each class in each task. Fig. B.1a shows a t-SNE (Maaten and Hinton, 2008) plot for the 16-dimensional weights. We see that when reduced to 2-dimensions, the weights cluster according to class. Fig. B.1b visualizes the weights in their original space. In this plot, weights from the same class are grouped together, and clear similarity patterns are evident across the image, showing that weights from the same class have similar means across tasks. Fig. B.2 details the task weights in 2-dimensional space. Here, each pentagon represents the weight means learned for one training task, where the nodes of the pentagon are colored according to the class the weights represent. In Fig. B.2a we see that overall, the classes cluster in 2-dimensional space as well. However, there is some overlap (e.g., classes ‘1’ and ‘2’), and that for some tasks a class-weight may appear away from the cluster. Fig. B.2b shows the same plot, but only for tasks that contain both class ‘1’ and ‘2’. Here we can see that for these tasks, class ‘2’ weights are all located away from their cluster.

This implies that each class-weights are typically well-approximated as being independent of the task. However, if the model lacks capacity to properly assign each set of class weights to different regions of space, for tasks where classes from similar regions of space appear, the inference procedure will ‘move’ one of the class weights to an ‘empty’ region of the space.

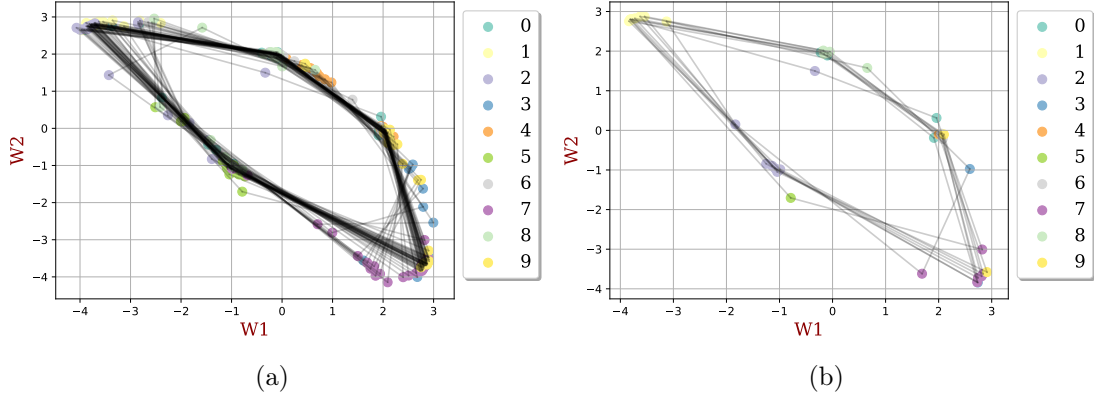


Figure B.2: Visualizing the task weights for $d_\theta = 2$. (a) All training tasks. (b) Only training tasks containing both ‘1’s and ‘2’s.

C. Comparing Training procedures and Forms of q for Few-Shot Classification (Omniglot)

We first derive a VI-based objective for our probabilistic model. For a single task t , an evidence lower bound (ELBO; (Wainwright and Jordan, 2008)) may be expressed as:

$$\mathcal{L}_t = \mathbb{E}_{q_\phi(\psi|D^{(t)}, \theta)} \left[\sum_{(x,y) \in D^{(t)}} \log p(y|x, \psi, \theta) \right] - \text{KL} \left[q_\phi(\psi|D^{(t)}, \theta) \| p(\psi|\theta) \right]. \quad (\text{C.1})$$

We can then derive a stochastic estimator to optimize Eq. (C.1) by sampling $D^{(t)} \sim p(D)$ (approximated with a training set of tasks) and simple Monte Carlo integration over ψ such that $\psi_l^{(t)} \sim q_\phi(\psi|D^{(t)}, \theta)$:

$$\hat{\mathcal{L}}(\theta, \phi) = \frac{1}{T} \sum_{t=1}^T \left(\sum_{(x,y) \in D^{(t)}} \left(\frac{1}{L} \sum_{l=1}^L \log p(y|x, \psi_l^{(t)}, \theta) \right) - \text{KL} \left[q_\phi(\psi|D^{(t)}, \theta) \| p(\psi|\theta) \right] \right), \quad (\text{C.2})$$

Eq. (C.2) differs from our objective function in Eq. (9) in two important ways: (i) Eq. (9) does not contain a KL term for $q_\phi(\psi|D^{(t)}, \theta)$ (nor any other form of prior distribution over ψ , and (ii) Eq. (C.1) does not distinguish between training and test data within a task, and therefore does not explicitly encourage the model to generalize in any way. To compare the two inference approaches, we train an identical model for few-shot classification on Omniglot (for experimental details see Section 4 and ??) using VI, and our approach with a Gaussian and δ -function form of q distribution. Results of this experiment are found in Table C.1.

Method	5-way		20-way	
	1-shot	5-shot	1-shot	5-shot
VERSA (δ -function, 1 sample)	99.24 \pm 0.16%	99.71 \pm 0.12%	97.24 \pm 0.19%	98.63 \pm 0.17%
VERSA (Gaussian, 1 sample)	99.26 \pm 0.14%	99.63 \pm 0.12%	97.19 \pm 0.20%	98.59 \pm 0.17%
VERSA (Gaussian, 10 samples)	99.28 \pm 0.15%	99.63 \pm 0.12%	97.27 \pm 0.19%	98.56 \pm 0.18%
VI (Gaussian, 1 sample)	93.76 \pm 0.30%	93.89 \pm 0.33%	90.29 \pm 0.24%	90.01 \pm 0.26%
VI (Gaussian, 10 samples)	93.70 \pm 0.26%	93.95 \pm 0.26%	90.09 \pm 0.22%	90.02 \pm 0.23%

Table C.1: Accuracy results for different few-shot settings on Omniglot. The \pm sign indicates the 95% confidence interval over tasks using a Student’s t-distribution approximation.

Table C.1 demonstrates that both forms of our framework significantly out-perform plain VI in this setting. We speculate that this is due to both the distinction between training and test

data and the detrimental effect of the KL term on held-out accuracy. We further see that for this case, both forms of q in our framework perform equally well, implying that uncertainty in ψ is not required for achieving good accuracy rates.

D. Experimentation Details

D.1. Few-shot Classification Network Architectures

Tables D.1 to D.3 detail the neural network architectures for the feature extractor θ , amortization network ϕ , and linear classifier ψ , respectively. The feature extraction network is very similar to that used in (Vinyals et al., 2016). The output of the amortization network yields mean-field Gaussian parameters for the weight distributions of the linear classifier ψ . When sampling from the weight distributions, we employ the local-reparameterization trick (Kingma et al., 2015), that is we sample from the implied distribution over the logits rather than directly from the variational distribution. To reduce the number of learned parameters, we share the feature extraction network θ with the pre-processing phase of the amortization network ψ .

Shared Feature Extraction Network (θ): $\tilde{x} \rightarrow h_\theta(\tilde{x})$

Output size	Layers
$28 \times 28 \times 1$	Input image
$14 \times 14 \times 64$	conv2d (3×3 , stride 1, SAME, RELU), dropout, pool (2×2 , stride 2)
$7 \times 7 \times 64$	conv2d (3×3 , stride 1, SAME, RELU), dropout, pool (2×2 , stride 2)
$4 \times 4 \times 64$	conv2d (3×3 , stride 1, SAME, RELU), dropout, pool (2×2 , stride 2)
$2 \times 2 \times 64$	conv2d (3×3 , stride 1, SAME, RELU), dropout, pool (2×2 , stride 2)
d_θ	fully connected, RELU

Table D.1: Feature extraction network used for Omniglot and *miniImageNet* few-shot learning. Omniglot uses dropout with a keep probability of 0.9 while *miniImageNet* uses 0.5. Batch normalization is used throughout.

Amortization Network (ϕ): $x_1^c, \dots, x_{k_c}^c \rightarrow \mu_{w^{(c)}}, \sigma_{w^{(c)}}^2$

Phase	Output size	Layers
feature extraction	$k \times d_\theta$	shared feature network (θ)
ϕ_{pre}	$k \times d_\theta$	fully connected, Linear
instance pooling	$1 \times d_\theta$	average
ϕ_{post}	$1 \times d_\theta$	$2 \times$ fully connected, ELU
ψ weight distribution	d_θ	fully connected linear layers to $\mu_{w^{(c)}}, \sigma_{w^{(c)}}^2$

Table D.2: Amortization network used for Omniglot and *miniImageNet* few-shot learning.

Linear Classifier (ψ): $h_\theta(\tilde{x}) \rightarrow p(\tilde{y}|\tilde{x}, \theta, \psi_t)$

Output size	Layers
d_θ	Input features
C	fully connected, softmax

Table D.3: Linear classifier used used for Omniglot and *miniImageNet* few-shot learning.

D.2. Few-shot Classification Accuracy Results

Table D.4 and Table D.5 provide numerical few-shot classification results for VERSA and competitive approaches.

Method	5-way		20-way	
	1-shot	5-shot	1-shot	5-shot
Siamese nets (Koch et al., 2015)	97.3%	98.4%	88.1%	97.0%
Matching Nets (Vinyals et al., 2016)	98.1%	98.9%	93.8%	98.5%
Neural Statistician (Edwards and Storkey, 2017)	98.1%	99.5%	93.2%	98.1%
memory mod (Kaiser et al., 2017)	98.4%	99.6%	95.0%	98.6%
MAML (Finn et al., 2017)	98.7 ± 0.4%	99.9 ± 0.1%	95.8 ± 0.3%	98.9 ± 0.2%
Prototypical Networks (Snell et al., 2017)	98.8%	99.7%	96.0%	98.9%
Reptile (Nichol and Schulman, 2018)	97.68 ± 0.04%	99.48 ± 0.06%	89.43 ± 0.14%	97.12 ± 0.32%
VERSA	99.24 ± 0.16%	99.71 ± 0.12%	97.24 ± 0.19%	98.63 ± 0.17%

Table D.4: Accuracy results for different few-shot settings on Omniglot. The ± sign indicates the 95% confidence interval over tasks using a Student’s t-distribution approximation.

Method	5-way	
	1-shot	5-shot
Matching Nets (Vinyals et al., 2016)	46.6%	60.0%
Meta LSTM (Ravi and Larochelle, 2017)	43.44 ± 0.77%	60.60 ± 0.71%
MAML (Finn et al., 2017)	48.7 ± 1.84%	63.11 ± 0.92%
Prototypical Networks (Snell et al., 2017)	49.42 ± 0.78%	68.20 ± 0.66%
Reptile (Nichol and Schulman, 2018)	49.97 ± 0.32%	65.99 ± 0.58%
VERSA	50.70 ± 0.86%	65.03 ± 0.66%

Table D.5: Accuracy results for different few-shot settings on *mini*ImageNet. The ± sign indicates the 95% confidence interval over tasks using a Student’s t-distribution approximation.

D.3. View Reconstruction Network Architectures

Tables D.6 to D.8 describe the network architectures for the encoder, amortization, and generator networks, respectively.

ShapeNet Encoder Network (ϕ): $y \rightarrow h$

Output size	Layers
$28 \times 28 \times 1$	Input image
$14 \times 14 \times 64$	conv2d (3×3 , stride 1, SAME, RELU), pool (2×2 , stride 2)
$7 \times 7 \times 64$	conv2d (3×3 , stride 1, SAME, RELU), pool (2×2 , stride 2)
$4 \times 4 \times 64$	conv2d (3×3 , stride 1, SAME, RELU), pool (2×2 , stride 2)
$2 \times 2 \times 64$	conv2d (3×3 , stride 1, SAME, RELU), pool (2×2 , stride 2)
d_ϕ	fully connected, RELU

Table D.6: Encoder network used for ShapeNet few-shot learning. No dropout or batch normalization is used, but otherwise this network is identical to the feature extraction network used in few-shot classification.

ShapeNet Amortization Network $(\phi): x_1^{(t)}, \dots, x_k^{(t)}, y_1^{(t)}, \dots, y_k^{(t)} \rightarrow \mu_\psi, \sigma_\psi^2$

Phase	Output size	Layers
ϕ_{pre}	$k \times d_\phi$	encoder network (ϕ)
concatenate h and X	$k \times (d_\psi + d_X)$	concat(h, X)
ϕ_{mid}	$k \times d_\phi$	2×2 fully connected, ELU
instance pooling	$1 \times d_\phi$	average
ϕ_{post}	$1 \times d_\phi$	$2 \times$ fully connected, ELU
ψ distribution	d_ψ	fully connected linear layers to μ_ψ, σ_ψ^2

Table D.7: Amortization network used for ShapeNet few-shot learning.

ShapeNet Generator Network $(\theta): \tilde{x} \rightarrow p(\tilde{y}|\tilde{x}, \theta, \psi^{(t)})$

Output size	Layers
$d_\psi + d_x$	concat(ψ, x)
512	fully connected, RELU
1024	fully connected, RELU
$2 \times 2 \times 256$	reshape
$4 \times 4 \times 128$	deconv2d (3×3 , stride 2, SAME, RELU)
$8 \times 8 \times 64$	deconv2d (3×3 , stride 2, SAME, RELU)
$16 \times 16 \times 32$	deconv2d (3×3 , stride 2, SAME, RELU)
$32 \times 32 \times 1$	deconv2d (3×3 , stride 2, SAME, sigmoid)

Table D.8: Generator network used for ShapeNet few-shot learning. No dropout or batch normalization is used.

D.4. View Recovery Accuracy Results

Table D.9 provides numerical few-shot view recovery results for VERSA and a C-VAE.

Model	Chairs			Planes		
	NLL	MSE	SSIM	NLL	MSE	SSIM
C-VAE	0.650	0.0320	0.560	0.645	0.0208	0.779
VERSA	0.643	0.0173	0.727	0.640	0.00989	0.894

Table D.9: ShapeNet view reconstruction test results. The average negative log likelihood (NLL) is measured in bits per pixel. The average mean squared error (MSE) and the average structural similarity index (SSIM) (Wang et al., 2004) are measured between the generated and ground truth images. The averages are taken over 100 randomly selected objects from the test set where 36 images uniformly spaced every 10 degrees in azimuth are generated from a single shot with the models.